(This is a sample cover image for this issue. The actual cover is not yet available at this time.)

Remote Sensing of Environment 124 (2012) 551–563

Contents lists available at SciVerse ScienceDirect

Remote Sensing of Environment

journal homepage: www.elsevier.com/locate/rse

The behaviour of mast-borne spectra in a snow-covered boreal forest

Kirsikka Niemi [a,d,*], Sari Metsämäki [a], Jouni Pulliainen [b], Hanne Suokanerva [b], Kristin Böttcher [a], Matti Leppäranta [c], Petri Pellikka [d]

[a] Finnish Environment Institute, P.O. Box 140, 00251 Helsinki, Finland
[b] Finnish Meteorological Institute, Arctic Research, Tähteläntie 62, 99600 Sodankylä, Finland
[c] Department of Physics, University of Helsinki, P.O. Box 48, 00014 Helsinki, Finland
[d] Department of Geosciences and Geography, University of Helsinki, P.O. Box 64, FI-00014 Helsinki, Finland

ARTICLE INFO

Article history:
Received 9 December 2011
Received in revised form 16 May 2012
Accepted 4 June 2012
Available online xxxx

Keywords:
Reflectance spectra
Scene reflectance
NDSI
Boreal forest
Snow mapping
SCA
MODIS

ABSTRACT

Forest canopy impairs the detection of snow underneath and optical interpretation methods tend to underestimate the snow coverage. The effect of measurement conditions on snow reflectance is considerably well understood, but the sensitivity of scene reflectance (when forest canopy present) to these properties is less examined. To investigate scene reflectance of a boreal forest, an Analytical Spectral Devices (ASD) Field Spec Pro JR was installed at the top of a 30-metre-high mast in Sodankylä, Northern Finland. Two sites – sparse forest and a forest opening – were monitored. The data consists of average reflectance spectra in the range 350–2500 nm, as well as of simultaneously acquired digital images. The Moderate Resolution Imaging Spectroradiometer (MODIS) is widely used for the monitoring of snow-covered area (SCA). Therefore, ASD spectra were resampled to the spectral characteristics of MODIS. Time series of normalised difference snow index (NDSI), normalised difference vegetation index (NDVI) and the reflectance at selected wavelengths were investigated in order to understand their behaviour in a snow-covered forest in spring. In order to discriminate between the effects of illumination conditions and the actual snow characteristics, reflectance spectra were measured both under direct and diffuse illumination. A specific focus was on the behaviour of NDSI, which is typically used in SCA retrieval – e.g. in MODIS snow mapping algorithms by NASA's Goddard Space Flight Center (GSFC). We further modelled the scene reflectance as a function of surface reflectances considering areal proportions of Scots Pines, shadowed snow and directly illuminated snow.
In the forest opening, NDSI was found to be relatively insensitive to illumination conditions, while in the forest stand it showed stronger dependence. This indicates that NDSI-based snow algorithms may provide a lower accuracy over forested areas. We demonstrated this by comparing the mast-observed indices and reflectances with the corresponding thresholds applied in MODIS snow mapping. The current thresholds led to underestimated snow cover in our test forest. It was also noticed that over the forest stand, variations in snow reflectance induced particularly great variation in the scene reflectance, even though visible snow-covered ground accounted for only half of the observed area as a result of the blocking effect of the trees. Comparison between the mast-borne and the modelled scene reflectance suggest that the surface reflectance observations could offer a feasible means to predict scene reflectance characteristics of snow-covered boreal forests observed by space-borne instruments.

1. Introduction

The overall goal of this study is to aid remote sensing methodology development in order to provide more reliable information on snow cover in boreal forest. From many points of view, it is necessary to produce frequent and spatially well-distributed information on snow cover. *In situ* data from snow-covered areas are limited, which emphasises the need to develop satellite methods for snow mapping. A good example is hydrological forecasting, which increasingly combines remote sensing data with hydrological models (Haefner et al., 1997; Solberg & Andersen, 1994; Winther & Hall, 1999). This information is valuable for flood prediction, hydropower industry and agriculture. In addition, seasonal snow cover is a sensitive indicator of climate change. Several climate models (e.g. Gong et al., 2007; Jylhä et al., 2004; Mellander et al., 2007) have predicted that climate change will considerably affect the boreal forest zone, where seasonal snow covers extensive areas in winter.

The reflectance of a scene observed by a satellite sensor is contributed by the reflectances of different targets. Snow differs considerably from other targets in its high reflectivity at visible and near-infrared (NIR) wavelengths. Bare ground and vegetation reduce the reflectance of a pixel containing snow. Therefore, the areal proportion of

* Corresponding author at: Finnish Environment Institute, P.O. Box 140, 00251 Helsinki, Finland. Tel.: +358 400 148 610 (mobile); fax: +358 9 5490 2690.
E-mail address: kirsikka.niemi@environment.fi (K. Niemi).

0034-4257/$ – see front matter © 2012 Elsevier Inc. All rights reserved.
doi:10.1016/j.rse.2012.06.008

these targets can be utilised for estimating the fraction of snow-covered area (Vikhamar & Solberg, 2003b). Optical remote sensing methods for estimating the areal extent of snow cover in boreal forest have been increasingly studied (e.g. Hall & Riggs, 2007; Hall et al., 1995; Klein et al., 1998; Metsämäki et al., 2005, 2012; Salminen et al., 2009; Salomonson & Appel, 2004; Vikhamar & Solberg, 2003a), but there is still a lack of information on the effect of coniferous forest on the scene reflectance. The forest canopy impairs the detection of snow underneath and remote sensing methods consequently tend to underestimate the snow coverage (Hall et al., 1998; Metsämäki et al., 2002, 2012; Vikhamar & Solberg, 2003b; Xin et al., 2012). In addition, the reflectance of snow itself varies depending on impurities, liquid water content, and grain size (Dozier et al., 2009; Hendriks & Pellikka, 2004; Painter et al., 1998, 2003; Pellikka & Rees, 2010; Warren, 1982), thus creating variations in scene reflectance. The exceptional reflectance of snow has been utilised in several operational snow monitoring activities, such as fractional snow cover mapping for the Baltic Sea area with *SCAmod* (Metsämäki et al., 2005, 2012), and for retrieval of the global Moderate Resolution Imaging Spectroradiometer (MODIS) snow cover products by the NASA's Goddard Space Flight Center (GSFC) (Hall et al., 1995, 2002; Klein et al., 1998; Riggs et al., 2006). *SCAmod*, developed and operated by the Finnish Environment Institute (SYKE), provides the areal fraction of snow-covered terrain for a specified unit-area. It is based on a reflectance model where the reflectance of the target is expressed a function of fractional snow cover. The effective canopy transmissivity is used to describe the effect of forest canopy into the scene reflectance. *SCAmod* is applicable to different sensors and spectral bands; SYKE's operational snow mapping utilises MODIS Band 4 (555 nm) reflectance data. On the other hand, the binary MODIS snow algorithm SNOWMAP by GSFC (Riggs et al., 2006) is based on thresholding rules for the normalised difference snow index (NDSI), the normalised difference vegetation index (NDVI) and the reflectances of MODIS Band 2 (859.5 nm) and Band 4. It classifies the pixel as snow-covered or snow-free.

Typically satellite observations provide a spatial resolution of hundreds of metres, a varying footprint and a varying view zenith angle, which hampers the investigation of the effects of tree canopy and surface in varying conditions. To overcome these problems, an Analytical Spectral Devices (ASD) Field Spec Pro JR spectrometer was installed on the top of a 30-meters-high mast to provide data from two sites: 1) a forest and 2) a forest opening with tree shadows. For both of these 185 m^2 sized areas an average instantaneous reflectance spectrum and simultaneously acquired digital images are obtained on a daily basis. The dataset enables the investigation of the effect of trees, physical properties of snow and solar illumination geometry on the scene spectra. Since the MODIS algorithm and *SCAmod* use spectral bands provided by MODIS, similar spectral bands were resampled from the ASD reflectance spectra. The evolution of NDSI, NDVI and single band reflectances throughout the spring were investigated with the time series from the forest and forest opening. Emphasis was given to the identification of the main variables affecting the spectral signal of snow-covered forest. Our hypothesis was that the spectra observed under direct illumination are likely to be sensitive to illumination geometry, while spectra observed under diffuse illumination should be more sensitive to the actual snow characteristics. Since NDSI was found to be a sensitive parameter to illumination and snow conditions, the applicability of MODIS snow mapping algorithms by GSFC was tested in the forest stand. Finally we investigated how the scene reflectance can be modelled using at ground observed spectra and areal proportions of forest stand with shadows and directly illuminated snow. The linear modelling of mast-borne spectra was earlier demonstrated by Salminen et al. (2009), but they limited their research to mast-borne measurement on a single day. In this article, the mast-borne data covers dozens of days. We also found that the effective transmissivity needs to be taken into account in the model. If the behaviour of snow-covered forest can be modelled in our test site, the model could be adapted to work in different kinds of forests as well.

2. The data set and study area

2.1. Study area

The study site is located in Sodankylä, Northern Finland at 26.6° E 67.4° N, about 100 km north of the Arctic Circle and 180 m above the sea level. The mast spectrometer monitors a Scots Pine forest and a three-shadowed forest opening (Fig. 1). Lichen and mosses on mineral soil characterize the ground layer (images of the areas are presented in the Section 3). The site represents seasonally snow-covered northern boreal forest. 92% of southern Lapland forests are dominated (fraction of pines >75%) by Scots Pines (METLA, 2010). Table 1 summarizes the key forest characteristics of the site and compares statistics of these variables to boreal forests of Northern Finland.

Snow typically covers the Sodankylä area from the end of October to the middle of May. The solar elevation is low throughout the year, with an annual maximum in midsummer of 46°. Because of the limited light conditions, optical satellite images are not practically usable from November until the middle of February. The winter is cold and long, making the snow cover rather homogenous. Wind is the main factor causing metamorphosis in the surface layer. Melt-freeze metamorphosis starts during the melting period in late spring causing a layered structure of the snow pack with ice lenses. During spring, the solar elevation and the length of the day increase quickly inducing a rapid snow melt. In Northern Finland, the average annual snow water equivalent is usually as high as 140–200 mm and the rapid melt may cause flooding during spring (Kuusisto, 1984).

2.2. Mast-borne spectrometer data

The mast is maintained by the Arctic Research Centre of the Finnish Meteorological Institute (FMI-ARC). The data consist of instantaneous average reflectance spectra from an area of 185 m^2 from a forest area and from a forest opening with tree shadows. In this paper, the average reflectance of the target area is denoted as scene reflectance. Scene reflectance measurements were made with an ASD Field Spec Pro JR spectrometer (ASD Inc., Boulder, Co, USA) installed at the top of a 30-metre-high mast (Fig. 1 left). The spectral range of the instrument is 350–2500 nm with a spectral resolution of 1.4 nm for 350–1000 nm and of 2 nm for 1000–2500 nm. The wavelengths beyond 1800 nm were not included in this study because of the low signal-to-noise ratio. The detector is at the end of an adjustable six-metre-long rotating pole and is tilted 11° from nadir. The field of view (FOV) of the utilised foreoptic is 25°. The incoming radiation is determined by measuring the radiance from a calibrated white Spectralon pane right after the target measurement, on average 30 s later. The radiance of the forest area is measured when the sensor azimuth is 110°, and the radiance from the forest opening is measured when the sensor azimuth is 270°. The average reflectance from the target scene at a particular wavelength $R_{Scene}(\lambda)$ was determined by:

$$R_{Scene}(\lambda) = R_{CAL}(\lambda) * \frac{L_{REF}(\lambda)}{L_{CAL}(\lambda)} * \frac{L_{Scene}(\lambda)}{L_{Ref}(\lambda)}, \quad (1)$$

where R_{CAL} is the instrument background noise, $L_{REF}(\lambda)$ is the radiance of the white Spectralon panel from the mast, $L_{CAL}(\lambda)$ is the radiance of the new white Spectralon panel, measured with $L_{REF}(\lambda)$ in the laboratory, $L_{Scene}(\lambda)$ is the measured average radiance from the target area, and $L_{Ref}(\lambda)$ is the radiance of the white Spectralon panel of the mast at the time of measurement. In addition, the digital camera acquires simultaneously images from the target area, enabling the determination of target characteristics at the time of the measurement, including e.g. the snow patchiness and the areal proportions of forest canopy, tree shadows, and directly illuminated snow. During the full snow cover at spring, average areal fractions for Pine, shadowed snow and directly illuminated snow in forest were 48%, 44% and 8%, respectively. In

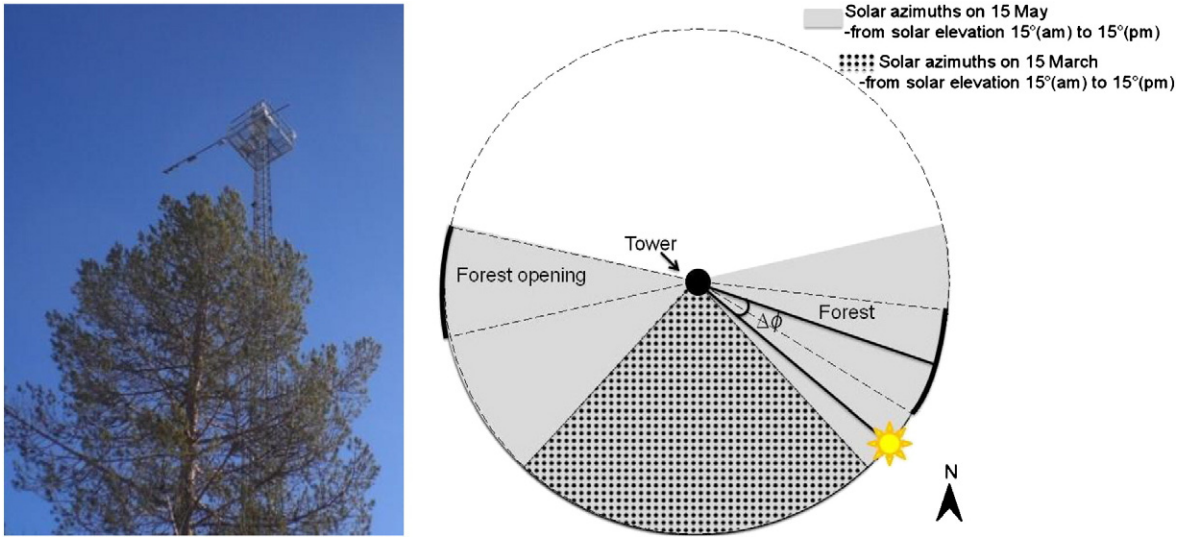

Fig. 1. Left: The ASD Field Spec Pro JR spectrometer installed on the top of 30-metre mast in Sodankylä, Northern Finland. Right: Field of view of the forest area and the forest opening as well as solar azimuths between solar elevation 15° (am) and 15° (pm). $\Delta\phi$ defines the azimuth angle difference between the instrument look angle and the sun.

open area, shadowed snow covered up to 84% and directly illuminated snow 16% on average. The mast-borne spectrometer set-up is described in more detail by Sukuvaara et al. (2007).

The period of interest is from March to May, providing appropriate illumination conditions and representative snow coverage. During that period, measurements from the forest site covered 46 days in 2010 and 56 days in 2011. Measurements from the forest opening were used only from year 2011 (55 days). The cases with very low solar elevation angle ($\theta < 15°$) were removed. In addition, to ensure a proper calibration, only measurements from either direct (i.e., clear sky: 0/8 to 2/8 cloud cover) or diffuse (i.e., cloudy sky: 7/8 to 8/8 cloud cover) solar illumination conditions were selected. Measurements under direct and diffuse illumination are studied separately. If several measurements were available within a time interval of 5 min, an average of these measurements was taken. In all, 116 measurement cases from the forest opening and 358 measurement cases from the forest area were investigated.

2.3. Ground-based measurements

An automatic thermometer (Pt100) next to the mast measures the snow surface temperature every minute. It is positioned at the snow surface level and is re-positioned according to the changing snow depths on daily basis. This information was used in the determination of snow wetness at the time of each mast-borne measurement. An ultrasonic ranging sensor (SR50-45) is situated near the mast, automatically providing snow depth measurements every minute. From these measurements, average snow depths at 10 min intervals were employed in the investigations. In addition, ground-based field spectrometer measurements were acquired for the modelling of the scene reflectance spectra. These data have been collected from the Sodankylä area since 2006 (Salminen et al., 2009). These include hundreds of reflectance spectra in a 350–2500 nm spectral range, measured with a portable ASD Field Spec Pro JR spectrometer, similar to the mast-borne spectrometer. The same measurement pattern was used in each case. The instrument foreoptic unit was set to look at nadir direction (sensor view angle 0°), which differs 11° from the mast spectrometer foreoptic. The angular FOV corresponds to that of the mast-borne spectrometer. The mean distance from FOV to target was 45 cm, and the view covered a surface area 20 cm in diameter. Measurements were made from directly illuminated snow and from shadowed snow in different weather conditions. Relevant information, such as weather conditions and physical properties of the snow layer, were filed with each spectrum. In addition, digital photographs of the snow sample, cloudiness, and landscape were taken for each measurement location. Only measurements with a clean, over 35 cm deep snow layer and a landscape similar to the location of the mast-borne spectrometer were exploited (see Table 2). Similarly to mast-borne observations, an average of the measurements within 5 min interval represents one measurement (typically at least 30 measurements are conducted within 5 min). In addition, reflectance spectra of Scots Pine twigs/small branches were measured in laboratory conditions. The elevation angle of light source was 35° corresponding to low Sun elevation angles in Sodankylä mast-borne snow measurements. These ASD ground-based reflectance measurements were used in the modelling of scene reflectance in Section 3.3.

Table 1
Forest characteristics in the study area and northern boreal forests of Finland.

	Test forest	Average in northern boreal forests[a]	Standard deviation in northern boreal forests[a]
Crown coverage (%)	40	30	10
Volume of growing stock (m^3/ha)	49	62	15
Median height (m)	11	12	5
Median trunk diameter at 1.3 m (m)	0.13	–	–
Crown thickness (m)	2.9	–	–

[a] Törmä et al., 2011.

3. Methodology

3.1. Time series analyses of scene reflectances related to MODIS-based bands and indices

In this study mast-borne spectrometer data were investigated using the bands and indices relevant to MODIS snow mapping algorithm

Table 2
Ground-based ASD measurements, which were applied in the modelling scene of reflectance.

Ground-based ASD measurements	Number of days	Measurement cases
Dry snow in direct light	5	16
Dry snow in shadow	4	10
Wet snow in direct light	4	8
Wet snow in shadow	2	4
Scots Pine branch	1	15

(Table 3) (Klein et al., 1998). For the resampled spectrometer bands, the naming convention corresponding to MODIS is used, see Table 3.

To investigate the behaviour of scene reflectances and indices in a snow-covered boreal forest during the melting period, time series of ASD measurements were created for the year 2010 (forest site) and for the year 2011 (forest opening). These time series feature several variations governed by weather and illumination conditions as well as snow characteristics. Our hypothesis is that the reflectances observed under direct illumination are likely to be sensitive to illumination geometry, while reflectances observed under diffuse illumination should be more sensitive to the actual snow characteristics. To visualise trends in the time series, linear regression lines are presented for the periods before and after the appearance of the first snow-free patches. In addition to analysing the time series, the effect of illumination geometry on the scene reflectance from the forest site was evaluated using several spectra observed under different solar azimuths and elevations on 18 March 2010.

The effect of snow cover in the tree canopy on scene reflectance was investigated using observations from two dates, 18 and 21 March 2010. The measurement time was 10.05 UTC, the snow surface temperatures were about the same, and the sky was cloudless on both days, but on the earlier day the trees were snow-free, while on the latter day they were partly snow-covered (Fig. 2).

3.2. Demonstration of the MODIS snow mapping techniques in the test forest

The observed scene reflectance from the forest area was used for evaluating the performance of the binary MODIS snow algorithm SNOWMAP (Hall et al., 1998; Klein et al., 1998; Riggs et al., 2006) and the fractional MODIS snow algorithm (Salomonson & Appel, 2004, 2006). SNOWMAP algorithm labels a pixel as snow-covered if the following criteria are met: 1) Band 4 >0.1, 2) Band 2 >0.11, and 3) NDSI ≥0.4. In addition, a pixel is labelled as snow-covered if it has NDSI and NDVI values within a certain range taking into account the forest cover of the pixel (Hall et al., 1998; Klein et al., 1998; Riggs et al., 2006). The applicability of the threshold values to the northern boreal forest was investigated with the mast-borne spectrometer observations acquired for full snow cover conditions with a snow depth higher than 40 cm, and with direct illumination.

The MODIS fractional snow product in “MOD10_L2” (Riggs et al., 2006) is based on the equations introduced by Salomonson and Appel (2006). Two resulting equations are applied; the one is based on the use of Terra/MODIS and the other on the use of Aqua/MODIS data. In this study, the Terra/MODIS algorithm was tested employing the mast-borne observations of reflectance over the test forest site as input to the algorithm. Accordingly, the fractional snow cover (FSC) was calculated as follows:

$$FSC = -0.01 + 1.45 * NDSI \quad (2)$$

In order to tentatively assess the feasibility of the current thresholds applied by MODIS snow algorithms in a resolution of MODIS 500 m data, we also investigated the MODIS-derived NDSI from dense forest canopy and the corresponding MODIS MOD10_L2 binary and fractional products distributed by the National Snow and Ice Data Center (NSIDC). This was carried out for a specific day with full snow cover conditions over the area of one Landsat/ETM+ sub-scene covering very dense forests along the Finnish–Russian border. This part of the work aimed at obtaining a preliminary idea of the method performance, without going into detailed investigations.

Table 3
Resampled reflectance bands and indices from mast-borne spectra.

MODIS bands	Central wavelength (nm)	Bandwidth (nm)
Band 1	645	620–670
Band 2	858.5	841–876
Band 4	555	545–565
Band 6	1640	1628–1652
MODIS-based indices	**Formulation**	
NDSI	(Band 4 − Band 6)/(Band 4 + Band 6)	
NDVI	(Band 2 − Band 1)/(Band 2 + Band 1)	

3.3. Modelling of scene spectra from ground-based spectrometer measurements

To relate the observed scene reflectance to the at-ground reflectance observations of snow and tree canopy (Table 2), a combination of linear mixing model and the zeroth-order solution of the radiative transfer equation was employed. The radiative transfer approach is applied to consider the effects of the forest canopy. The combined model expresses the scene reflectance as a function of the at-ground reflectances and their areal proportions while also accounting for the forest transmissivity (t) as an important parameter. It follows the reflectance model employed in the *SCAmod* approach for the mapping of fractional snow-covered area (Metsämäki et al., 2005, 2012). However, here the model is divided into two major terms: one accounting for the area of directly illuminated snow and another accounting for forest canopy comprising the trees and their casted shadows. The areal fractions for directly illuminated snow ($F_{ill.snow}$) and for the forest canopy ($1-F_{ill.snow}$) could be determined from high-resolution digital images for each measurement separately, see Fig. 3. The model gives the scene reflectance $R_{Scene}(\lambda)$ for this specific site as follows:

$$R_{Scene}(\lambda) = F_{ill.snow}\rho_{ill.snow}(\lambda) + (1-F_{ill.snow})\left[t(\lambda)\rho_{shd.snow}(\lambda) + \left(1-t^2(\lambda)\right)\rho_{trees}(\lambda)\right] \quad (3)$$

where $\rho_{ill.snow}(\lambda)$ is the at-ground reflectance of directly illuminated snow at wavelength λ, $\rho_{shd.snow}(\lambda)$ is at-ground reflectance of shadowed snow and $\rho_{trees}(\lambda)$ is the reflectance of an opaque forest canopy, estimated from the reflectance measurements of Scots Pine branches at the laboratory conditions. The effective one-way transmissivity $t(\lambda)$ describes the canopy's ability to transmit light and is related to the visibility of ground through the forest canopy from above. The last term $(1-t^2(\lambda))\rho_{trees}(\lambda)$ results from the zeroth-order solution of the radiative transfer equation. It includes the two-way transmissivity $t^2(\lambda)$ that is approximated by the square of one-way transmissivity (i.e. ignoring the effects of the viewing geometry). The solution of the radiative transfer equation also requires that $\rho_{trees}(\lambda)$ in Eq. (3) represents the reflection from an opaque forest canopy. In the forest opening site, transmissivity is equal to 1 and Eq. (3) reduces to:

$$R_{Scene}(\lambda) = F_{ill.snow}\rho_{ill.snow}(\lambda) + (1-F_{ill.snow})\rho_{shd.snow}(\lambda) \quad (4)$$

The ground-based measurements (Table 2) indicated that the reflectance spectra of wet snow are different from that of dry snow (see Fig. 4), which is in line with several studies (e.g. Dozier et al., 2009; Rasmus, 2005; Salminen et al., 2009; Warren, 1982). Therefore, the model was tested separately for measurements made under wet snow conditions (snow surface temperature T≥0 °C) and under dry snow conditions (T<0 °C). In both cases, the mean values for $\rho_{ill.snow}$ and $\rho_{shd.snow}$ were calculated from ground-based ASD measurements (see Table 2). Mean $F_{ill.snow}$ was calculated using mast-borne measurements under direct illumination and over 40 cm deep snow layer for both dry (52 measurement cases from forest, 12 from forest opening) and wet snow conditions (23 measurement cases from forest, 14 from forest opening). In addition, a third test was carried out based on the combined observations from these two categories i.e. applying averages of dry and wet snow spectra. In the last case, $F_{ill.snow}$, $\rho_{ill.snow}$ and $\rho_{shd.snow}$ were determined as a weighted average from at-

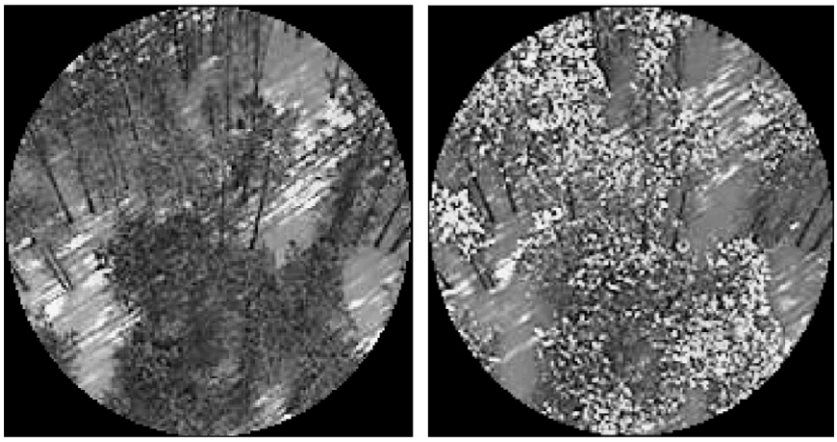

Fig. 2. The specific forest area of mast-borne ASD measurement. Left: On 18 March 2010 the trees were free from snow. Right: On 21 March 2010 the trees were covered by snow.

ground observed dry snow reflectance and from at-ground observed wet snow reflectance:

$$F_{ill.snow} = (F_{ill.snow}(dry) + F_{ill.snow}(wet))/2 \quad (5a)$$

$$\rho_{ill.snow} = (\rho_{ill.snow}(dry) + \rho_{ill.snow}(wet))/2 \quad (5b)$$

$$\rho_{shd.snow} = (\rho_{shd.snow}(dry) + \rho_{shd.snow}(wet))/2 \quad (5c)$$

The modelled spectrum was compared with the average of the all observed scene spectra which were measured in the corresponding snow conditions (i.e. dry, wet or weighted average of them), under direct illumination and with over 40 cm deep snow layer. As the transmissivity of the forest is *a priori* unknown, the constant values of transmissivity were estimated by fitting the model (3) into the scene reflectance spectra. In practise, the forest canopy transmissivity $t^2(\lambda)$ was separately estimated for three wavelength bands: 350–699 nm, 700–1349 nm, 1350–1800 nm. That is, a constant value of transmissivity was determined for each interval by minimizing the root mean square (rms)-difference between the model predictions and the observed hyper-spectral scene reflectance measurements. The use of separate vegetation canopy transmissivity values for these bands is justified by several earlier investigations that indicate distinct differences in plant tissue transmittance for these three bands (e.g. Knipling, 1970; Woolley, 1971; Zarco-Tejada et al., 2004).

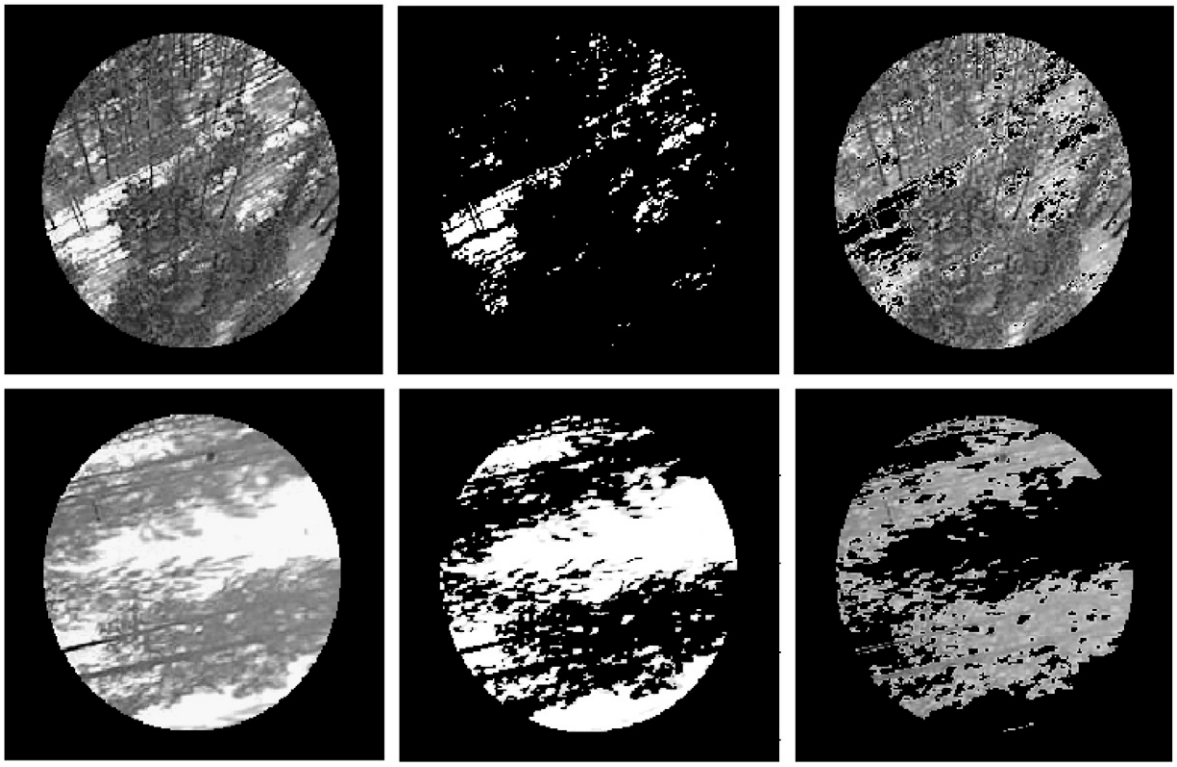

Fig. 3. Example cases of the image classification, which was done for each measurement separately to represent their individual conditions. (Above) Left: Digital image of the forest site observed by the mast-borne ASD spectrometer. Middle: Pixels classified as directly illuminated snow (9%), Right: The remaining pixels including trees and shadows (91%). (Below) Left: Digital image of the forest opening observed by the mast-borne ASD. Middle: Pixels classified as directly illuminated snow (51%), Right: Pixels classified as shadowed snow (49%).

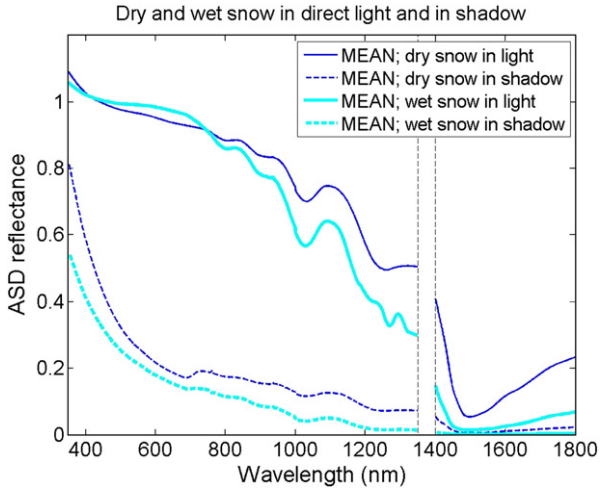

Fig. 4. The average reflectance spectra of dry and wet snow in direct light and in shadow. The measurements are described in Section 2.3. The wavelengths 1350–1400 nm are disturbed by a bad signal-to-noise ratio.

4. Results

4.1. The influence of prevailing conditions on scene reflectance from boreal forests

The time series of the resampled reflectance bands and indices for the forest opening (year 2011) are presented in Fig. 5 b–f, while Fig. 6 b–f presents the corresponding time series for the forest site (year 2010). The time series comprise each ASD-observation made within the time period in concern and the occasional multiple observations for a specific date are shown as scattered values for that date. The time series are presented separately for direct and diffuse illumination. In addition, time series for precipitation, snow depth, air temperature at 2 m and temperature at the ground are presented in Fig. 5a for year 2011 and in Fig. 6a for year 2010. These values, especially the snow depth, do not represent the actual values of the measured area but are measured in the vicinity of the mast. The digital images serve as the main information source of the snow cover. The average scene reflectances and indices at direct and diffuse illumination conditions from the forest opening and from the forest area are presented in Table 4, separately for wet and dry snow.

Both in the forest and in the forest opening, the reflectance was higher under diffuse illumination than in direct illumination, especially in wavelengths shorter than 1000 nm (Figs. 5b–d and 6b–d, Table 4). This is because under direct illumination shadows cast on snow decrease the reflectance. This phenomenon was more noticeable in the forest opening due to the dominance of snow reflectance where shadows give a clear contrast.

In the forest opening, the behaviour of NDSI was rather similar under direct and diffuse illumination; same goes for NDVI. This indicates that the indices were neither very sensitive to the solar illumination geometry nor to the amount of shadows in fully snow-covered areas (Fig. 5e and f). As to the reflectances under direct illumination, changes in illumination geometry caused clear variations. This can be seen e.g. on day 114 (24 April 2011), when several measurements during the cloud-free day were taken, leading to variation in reflectances. Generally, variance of the reflectances under direct illumination was higher compared to diffuse illumination, see e.g. coefficients of variation (CV) for wet snow in forest opening in Table 4. However, indices presented a more similar variation under both illumination conditions, again indicating their ability to compensate for the illumination geometry in open areas. The general trend of NDSI throughout the period shows a slight increase (Fig. 5e). This is due to the increasing grain size and liquid water content which rise as melting progresses, reducing reflectance more in the infrared region compared to the visible region (Fig. 5c and d). The negative correlation between grain size and snow reflectance in the infrared region has been found in many previous studies (Dozier et al., 2009; Nolin & Dozier, 2000; Painter et al., 1998; Warren, 1982). Notably different values for reflectances or indices according to the snow wetness were introduced only under diffuse illumination (Table 4); under direct illumination, large variation of illumination geometry compensated for the effect of wetness.

In the forest site, the behaviour of NDSI and NDVI under direct illumination differed clearly from that under diffuse illumination, indicating that the indices were sensitive to the solar illumination geometry in forest (Fig. 6e and f). For both indices, also the variation of values within a single day was notable and mainly caused by the varying illumination geometry, see e.g. day 77 (18 March 2010), providing 21 observations. Correlation coefficient r^2 between NDSI and the solar elevation angle was 0.65, while r^2 between NDSI and the solar azimuth angle was 0.52. The corresponding correlation coefficients for NDVI were 0.17 and −0.59, respectively. The reflectance spectra for that particular day are shown in Fig. 7. According to the figure, solar azimuth had a significant effect on the reflectance spectra, as the magnitudes of backscattered spectra (relative azimuth $\Delta\phi \geq 90°$, dashed curve) were clearly higher compared to those of forward scattered ones. This was particularly the case in the infrared region, and cannot be explained by the proportion of shadowed snow. No significant changes occurred in the area during that day; snow depth was 77 cm and temperature varied from −27 °C to −5 °C. This result is in line with earlier studies e.g. by Walter-Shea et al. (1997), Eklundh et al. (2007) and Peltoniemi et al. (2005) who demonstrated that vegetation reflects more in the backscattering direction compared to forward scattering direction. Throughout the whole period from the beginning of March to the end of April, NDSI and NDVI from the forest site showed a clear trend only in the case of direct illumination: NDSI increased while NDVI decreased (Fig. 6e and f). These trends are related to the increasing solar elevation during the period, as concluded e.g. by Gutman (1991) and Cao and Liu (2006).

The appearance of snow-free patches introduced different effects on the reflectance spectra of the forest site and forest opening. In the forest site, the digital images indicated that the first snow-free patches appeared around the trees on the day 118 (28 April 2010). No clear effect on either the scene reflectance or on the indices could be found (Fig. 6b–f), probably because the effect of vegetation (tree canopy) was already notable on spectra. From the day 131 (11 May 2010), the patches expanded rapidly, showing up an increasing fraction of snow-free ground in the measured area. This caused a sudden decrease of Band 2 and Band 4 reflectances and at the same time, an increase of Band 6 reflectance. Consequently, NDSI rapidly decreased while NDVI increased. Besides the increasing patchiness, the thinness of snow layer and the increasing impurities on snow decreases the visible reflectance. In the forest opening, the first snow-free patches appeared from the day 115 (25 April 2011). However, at that time, the snow pack is almost even, and the decreasing trend of Band 2 and Band 4 reflectance was partially caused by the thinning of the snow layer (after the patches snow depths can be assumed to be thin <20 cm). This is supported by the findings e.g. by Warren (1982) and Salminen et al. (2009). From the day 127 (7 May 2011), the patches expanded rapidly showing up an increasing fraction of vegetation in the measured area. This caused a sudden decrease of NDSI and an increase of NDVI. NDSI, in turn, showed lower dependence on the snow depth (Fig. 5e).

Snowfall is expected to affect the observed reflectances as well as the NDSI. In the forest opening, days 70 (11 March 2011) and 110 (20 April 2011) provided observations made right after a snowfall which deposited a layer of new snow. On both days, Band 6 reflectance suddenly raised while only slight increase in Band 2 and Band 4 reflectances was shown. This led to a strong decrease in NDSI (Fig. 5d

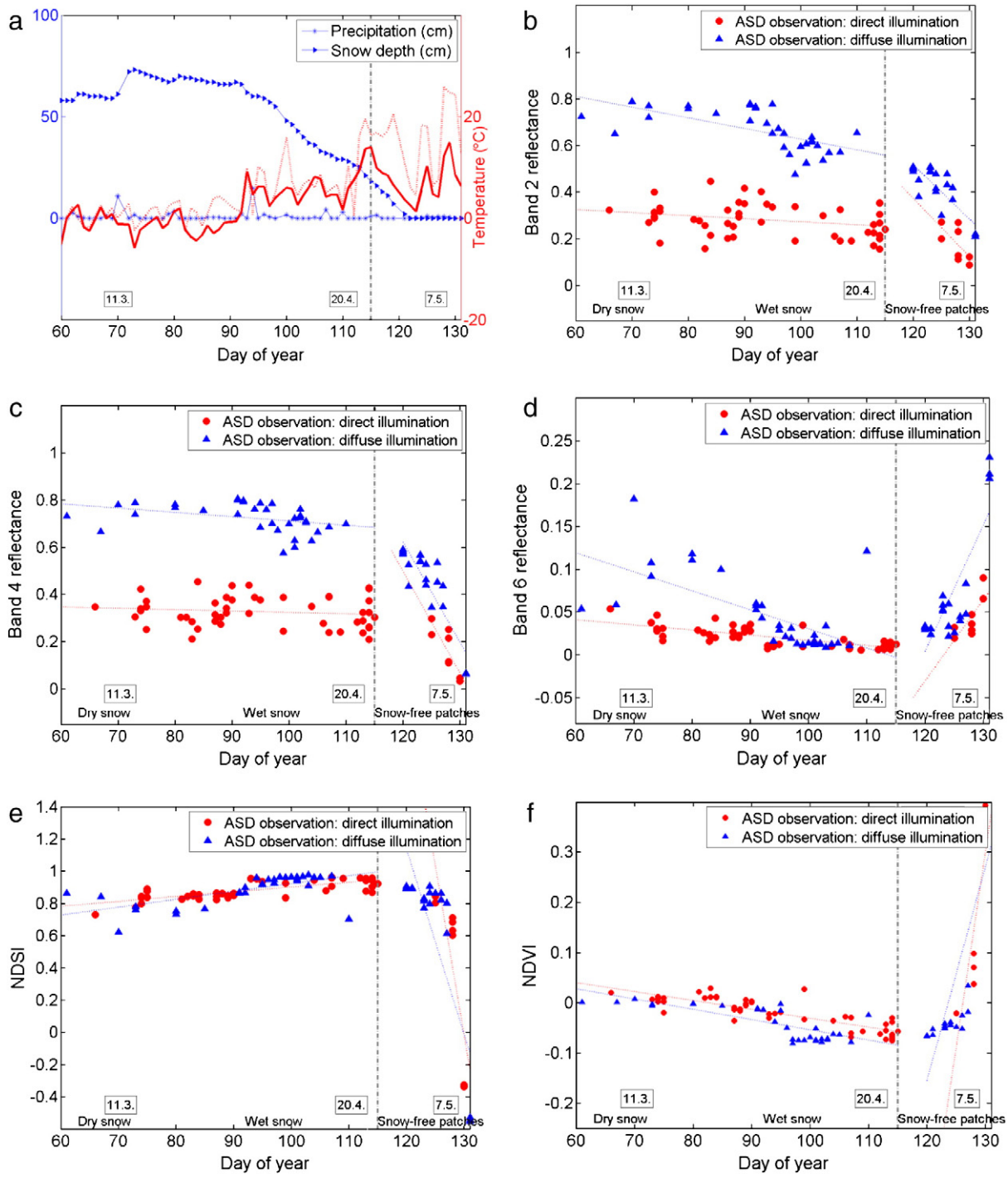

Fig. 5. Time series plots of forest opening measurements from 2 March 2011 to 11 May 2011. a) Precipitation, snow depth, air temperature at 2 m (bold line) and temperature at ground (dashed line), b) Band 2 scene reflectance, c) Band 4 scene reflectance, d) Band 6 scene reflectance, e) NDSI and f) NDVI as measured by the mast-borne spectrometer under direct or diffuse solar illumination. Under direct illumination, during the full snow cover shadowed snow covers on average 84% of the measurement footprint. Vertical dashed line indicates the appearance of snow-free patches.

and e). Evidently, this was caused by the small grain size of new snow (e.g., Marshall & Oglesby, 1994) which caused more variation in infrared region compared to visible region (Dozier et al., 2009; Nolin & Dozier, 2000; Painter et al., 1998; Warren, 1982). Negi et al. (2010) have also found a positive correlation between NDSI and snow grain size as well as between NDSI and the snow ageing. In the forest site, in turn, snowfall induced the NDSI to increase. This is because snow was intercepted by the canopy, and the increased proportion of snow visible to the sensor clearly increased the scene reflectance. This is seen when comparing the spectra from two days, the one with snow-free canopy and the other with snow-covered canopy. Snow cover on the trees caused tripling of the proportion of directly illuminated snow and over a 40% increase of the proportion of shadowed snow in the observation area; see Table 5. These had a considerable effect on the observed scene reflectance, especially in the visible region (Fig. 8). Snow on the canopy increased NDSI considerably, as

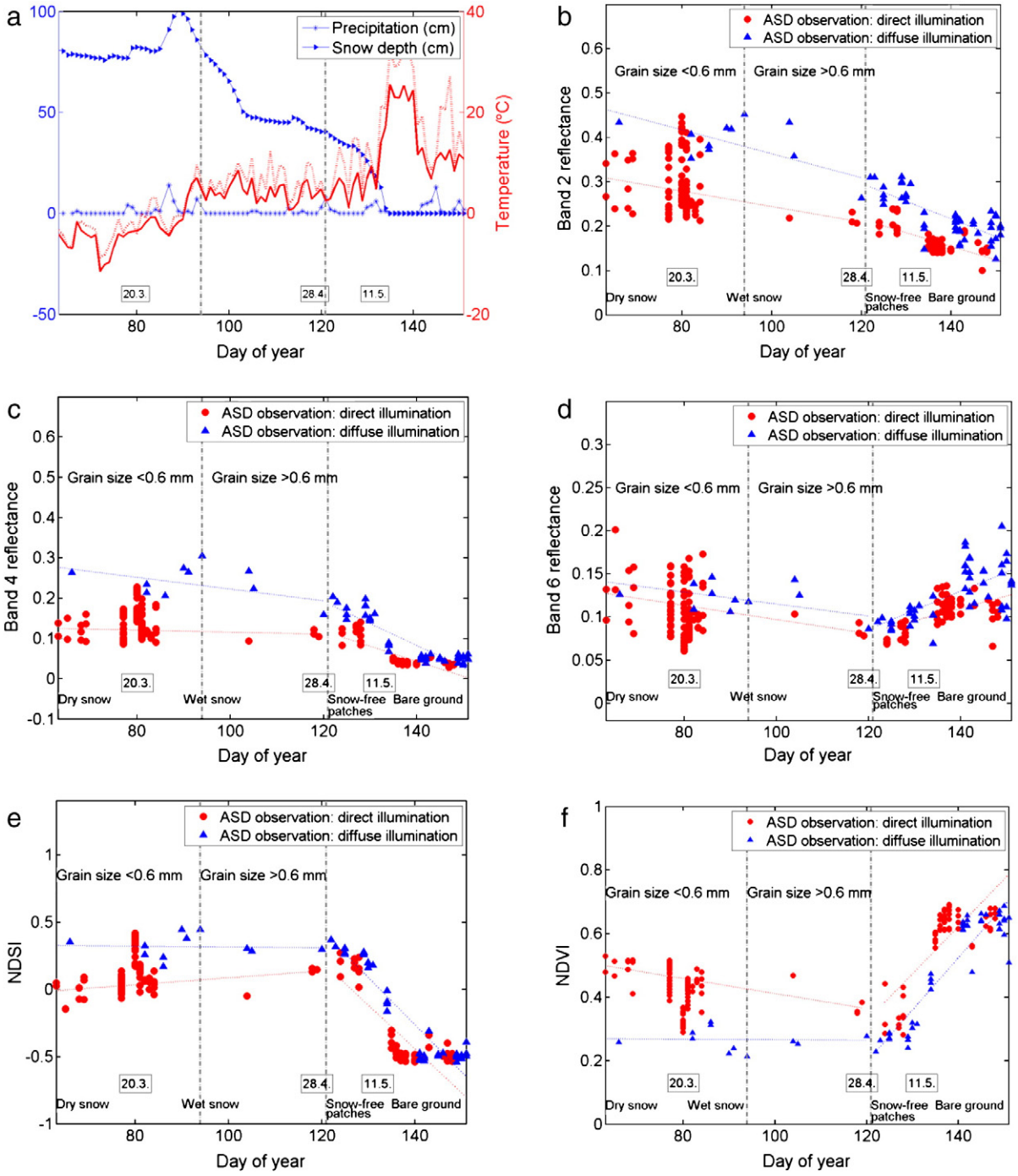

Fig. 6. Time series plots of forest measurements from 4 March 2010 to 31 May 2010. a) Precipitation, snow depth, air temperature at 2 m (bold line) and temperature at ground (dashed line), b) Band 2 scene reflectance, c) Band 4 scene reflectance, d) Band 6 scene reflectance, e) NDSI and f) NDVI as measured by the mast-borne spectrometer under direct or diffuse solar illumination. Under direct illumination, during the full snow cover shadowed snow covers on average 44% of the measurement footprint.

expected (see Table 5). The notable increase of NDSI from 0.05 to 0.40 implies that snow on canopy strongly affects the snow cover mapping either if the method is based on a single band reflectance like *SCAmod* or on band ratio like MODIS snow mapping algorithms.

4.2. Sources of error in snow cover mapping in a boreal forest

NDSI was found to be a sensitive variable especially in the forest site used in this study. This emphasizes the need for testing the NDSI-based techniques for the forest-covered scene. The MODIS SNOWMAP algorithm is based on the threshold values for Band 2 reflectance, Band 4 reflectance, NDSI and NDVI (Hall et al., 1998; Klein et al., 1998; Riggs et al., 2006). We applied the algorithm to mast-borne scene observations from the fully snow-covered (snow depth >40 cm) forest site as well as the forest site with patchy snow ($1<$snow depth ≤ 40 cm) and snow-free ground. Fig. 9 (left) presents the observations in NDSI-Band 4 space. The criterion for Band 2 is irrelevant in our case because it is used for capturing water areas. According to Fig. 9 (left), the threshold for NDSI did not capture the snow in the study area. Also Band 4 reflectances <0.1 were measured with full snow cover, which would be labelled as 'snow-free' according to the SNOWMAP algorithm. Fig. 9 (right)

Table 4
Reflectances and indices from forest area (snow depth >40 cm, snow-free trees, full snow cover) and forest opening (snow depth >25 cm, full snow cover) in dry and wet snow conditions under direct and diffuse illumination.

	No. of obs.	Band 2 (858.5 nm)		Band 4 (555 nm)		Band 6 (1640 nm)		NDSI		NDVI	
		Mean	CV	Mean	CV	Mean	CV	Mean	CV	Mean	CV
Forest opening											
Direct illumination											
Dry snow conditions	15	0.29	0.24	0.33	0.15	0.03	0.33	0.83	0.05	0	–
Wet snow conditions	25	0.28	0.21	0.33	0.21	0.02	0.50	0.90	0.06	−0.02	−1.50
Diffuse illumination											
Dry snow conditions	2	0.75	0.04	0.76	0.05	0.10	0.10	0.77	0.01	0	–
Wet snow conditions	30	0.65	0.14	0.72	0.09	0.04	0.85	0.91	0.07	−0.04	−0.74
Forest area											
Dry snow conditions	44	0.30	0.21	0.13	0.26	0.12	0.26	0.06	1.62	0.45	0.12
Wet snow conditions	38	0.26	0.17	0.13	0.23	0.09	0.18	0.15	0.69	0.40	0.14
Diffuse illumination											
Dry snow conditions	6	0.40	0.10	0.24	0.11	0.12	0.14	0.35	0.16	0.27	0.10
Wet snow conditions	40	0.39	0.13	0.27	0.21	0.10	0.26	0.43	0.35	0.21	0.31

presents all the observations in NDSI–NDVI space, with the acceptance region by Hall et al. (1998) and Klein et al. (1998) marked with grey. The fact that many observations (53%) fell outside this region indicates that the SNOWMAP algorithm cannot properly catch the snow-covered ground. Mainly this is due to the threshold for NDSI; also negative NDSI values were introduced. Even NDSI values as low as −0.15 were found with a full snow cover deeper than 70 cm. Xin et al. (2012) also found that NDSI can be negative even with snow on the ground, since the presence of forest can significantly decrease the green band reflectance. This is mainly due to the decrease of viewable gap fraction (VGF) within forest stand when observed at large view zenith angle and with low sun altitude.

The MODIS fractional snow algorithm (Riggs et al., 2006; Salomonson & Appel, 2004, 2006) was tested by applying Eq. (2) to the mast-based observations from forest site with full snow cover (snow depth >40 cm) and with partial snow cover (snow depth 1–40 cm). The derived FSC are presented in Fig. 10, indicating that FSC is strongly underestimated even with full snow cover (see also Metsämäki et al., 2012). Large variation occurs even within one day, depending on the sun elevation which affects the NDSI (Xin et al., 2012) and therefore the FSC. The results suggest that the consideration of illumination geometry would benefit the NDSI-based snow mapping.

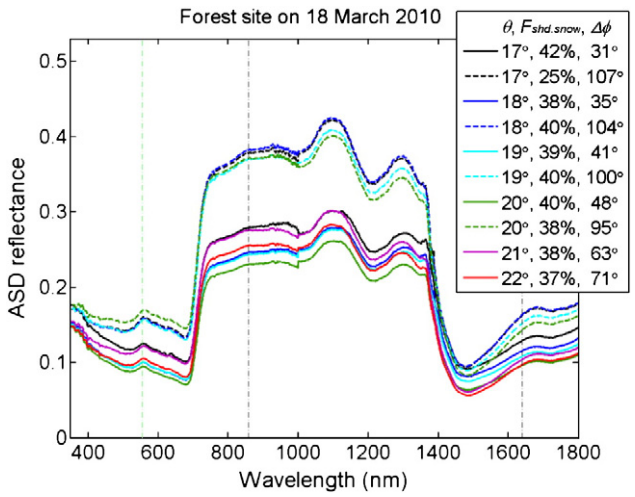

Fig. 7. The effect of solar elevation θ, fraction of shadowed snow $F_{shd.snow}$ and the relative azimuth $\Delta\phi$ on scene reflectance of forest area in dry snow conditions on 18 March 2010. The sun is in the direction of instrument view when $\Delta\phi = 0$. Dashed curves and solid curves represent backscattered and forward scattered spectra, respectively.

Forests in Finland are relatively sparse, but very dense forests are typical e.g. in Russia. It is evident that the problems related to the use of NDSI-based methods in the scale of mast-borne observations will arise also in the scale of MODIS 500 m-pixel. We demonstrate this for a forest area over Finnish–Russian border, see the subset of Landsat/ETM+ scene (186/017, 15 March 2003) in Fig. 11a) with dense forests depicted well along the border line in southwest-northeast direction (dark areas). We investigated the performance of MODIS MOD10_L2 v005 binary and fractional snow products for that area on 28 March 2003. Several weather station observations (Snow depth and snow coverage) as well as an SWE-map from Microwave radiometer data (from ESA DUE-GlobSnow, www.globsnow.info) indicate that the area – also forest floor – is fully snow-covered. This is supported also by the general climatology for that area. The ETM+ is of resolution 25 m × 25 m; the MODIS 500 m NDSI (Fig. 11b) illustrates that an individual forest patch may cover a whole MODIS-pixel. For this particular sub-scene with average view zenith angle ~32°, NDSI values for the most dense forests are very low, <0.1. Accordingly, MOD10_L2 V005 binary snow algorithm fails in identifying the snow properly (Fig. 11c). Also MOD10_L2 fractional snow product based on the NDSI shows clear underestimations (Fig. 11d). So we can deduce that in the scale of a MODIS-pixel a dense forest patch may introduce so low NDSI even with full snow cover, that binary method as well as fractional method may fail in snow identification.

4.3. Simulation of scene spectra

The effect of the tree canopy on scene reflectance spectra was investigated by applying the model given by Eq. (3) for the forest site

Table 5
The effect of snow on tree canopy to the scene spectrum: 18 March 2010 the trees were snow-free, while three days later they were snow-covered. Otherwise, conditions were similar on both days.

	18 March 2010 at 10:05 UTC	21 March 2010 at 10:05 UTC
Solar azimuth (°)	175.5	175.7
Solar elevation (°)	21.7	22.9
Snow depth (cm)	77	83
Grain size (mm)	0.54	0.38
Proportion of snow-free trees (%)	62.4	39.5
Proportion of directly illuminated snow (%)	3.8	11.9
Proportion of shadowed snow (%)	34.0	48.6
Snow surface temperature (°C)	−6	−7
Air temperature (°C)	−4	−5
NDSI	0.05	0.40
NDVI	0.51	0.32

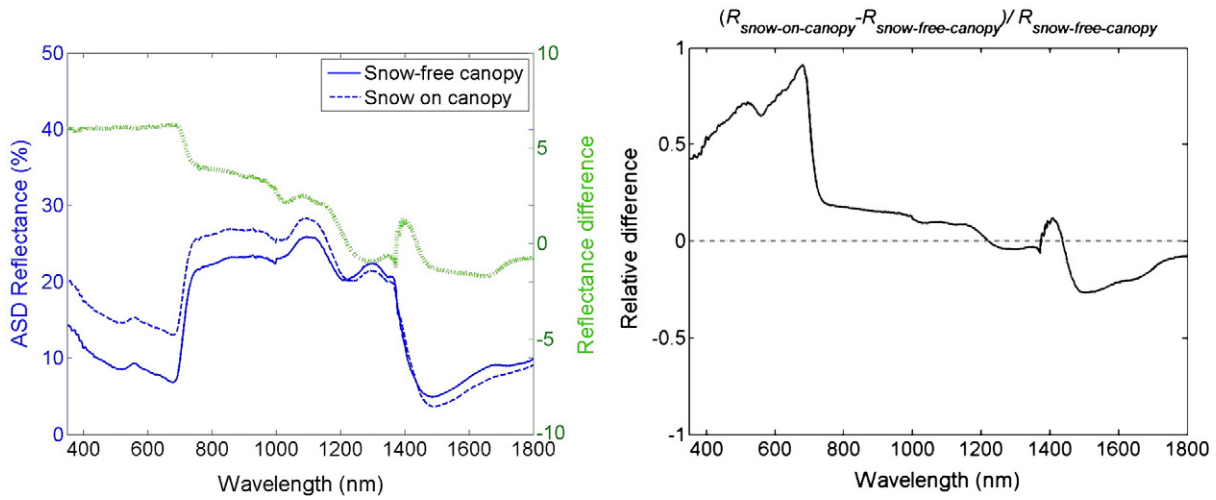

Fig. 8. The effect of snow on tree canopy to scene spectrum. On 18 March 2010 canopy was snow-free, while on 21 March 2010 the canopy was snow-covered. Left: Spectra from both days (blue line) and their difference (green line). Right: Relative difference between the spectra.

and Eq. (4) for the forest opening. As described in Section 3.3, the forest canopy transmissivity was determined for three wavelength intervals. The estimates for the transmissivity t were 0.04 for 350–699 nm, 0.78 for 700–1399 nm and 0.54 1400–1800 nm. The general behaviour of the estimated transmissivity is in agreement with the vegetation transmittance characteristics according to e.g. Knipling (1970), Woolley (1971), Mesarch et al. (1999) and Zarco-Tejada et al. (2004).

The simulated scene spectra was compared with the average observed reflectances, see Fig. 12. Observations and simulations correspond to direct illumination conditions, implying that also shadowed snow was present. In general, the model worked well in both areas. In the forest, the difference between modelled and observed spectra was greatest in the wavelength region around 750–1350 nm. In the forest opening, the model predicted a bit too high scene reflectances at the visible wavelengths, especially in dry snow conditions (Fig. 12b), while in NIR region a slight underestimation of scene reflectance was obtained.

For comparison, also a linear mixing model without the radiative transfer approach (i.e. without employment of forest transmissivity) was tested to simulate the observed scene reflectance spectra. However, this method could not adequately explain the behaviour of data without introducing purely empirical correction factors (see also Salminen et al. (2009) for the application of a linear mixing model for the Sodankylä mast-borne ASD measurements). The predicted reflectances with linear mixing model were too high in visible and NIR region indicating the underestimation of the effect of forest canopy on the snow reflectance beneath it.

5. Discussion and conclusions

In this article, the scene spectra from forest and forest opening in the visible and near-infrared domain was examined in order to improve the consideration of forest canopy effects in space-borne remote sensing of snow. The work was carried out using extensive time series of scene spectra measured by a mast-borne spectrometer system observing a forest area and a forest opening with tree shadows. In particular, the feasibility of two spectral indices, NDSI and NDVI was investigated and compared with spectral reflectances corresponding to MODIS bands. The results indicate that in open areas, NDSI and NDVI are able to reduce disturbances caused by variations in illumination geometry and snow depth, which induce large variation in reflectances. Thus, it is beneficial to apply these indices for snow mapping in sparsely vegetated or open areas, as in the case of the MODIS SNOWMAP algorithm. In forests, however, the

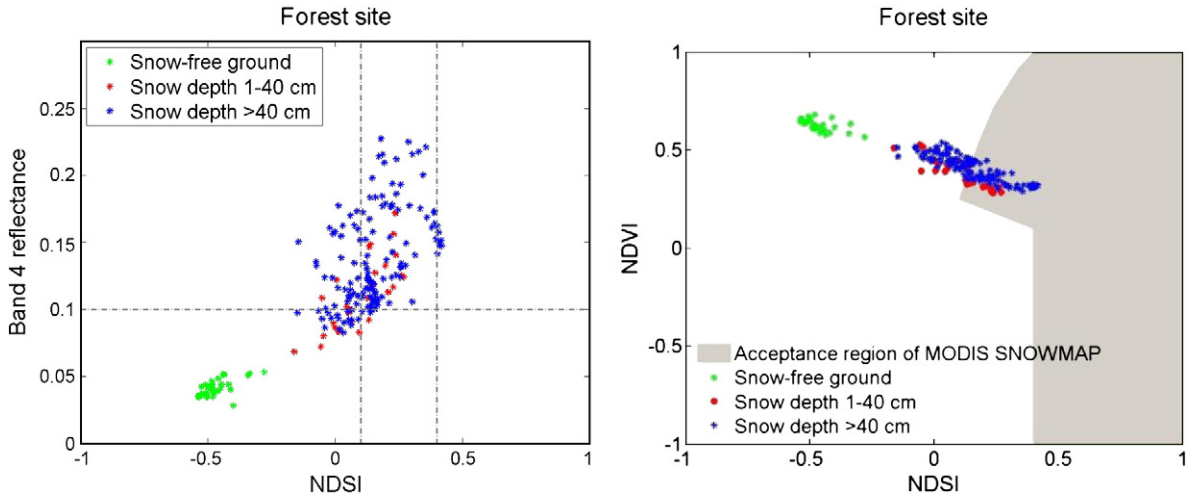

Fig. 9. Observations from the forest site as related to the criteria applied by the binary MODIS snow algorithm SNOWMAP. Left: observations in NDSI-Band 4 space. Vertical lines represent the outer limits of the NDSI acceptance area, while the actual NDSI-threshold is dependent on the NDVI. Right: The observed NDSI and NDVI with respect to the acceptance area employing NDVI, NDSI and Band 4 reflectance (criterion for band 2 for identifying water areas is irrelevant here).

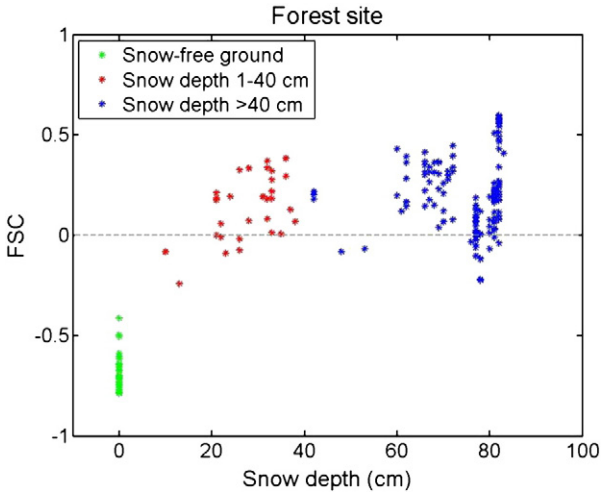

Fig. 10. The fractional snow cover (FSC) was calculated using the MODIS fractional snow algorithm (Riggs et al., 2006; Salomonson & Appel, 2004, 2006) with the scene reflectance observations from the forest site as input to the algorithm. Blue symbols represent full snow cover conditions in the forest site.

indices fluctuate strongly according to the illumination geometry, indicating that the improvements provided by spectral indices are marginal compared with single band reflectance.

Snow reflects more in a forward direction. However, the results obtained for varying illumination geometries indicate that the backscattered spectrum introduced by the tree canopy (crown coverage of 40%) dominates the scene spectra even with full snow-covered ground. This demonstrates that the forest canopy strongly affects the bidirectional reflectance observed from a target scene when compared with the observations from a snow-covered terrain without a forest canopy.

Investigation of the effect of snow cover on trees demonstrated that snowfall has a major impact on scene reflectance spectra and the spectral indices from boreal forest, especially on NDSI. NDSI was eight times higher when trees were snow-covered compared with snow-free trees. This was the case despite the smaller grain size of freshly fallen snow which theoretically should introduce lower NDSI (e.g. Negi et al., 2010). Concerning the effect of snow depth, the results suggest that reflectances at visible wavelengths may drop more considerably compared to NDSI with decreasing snow depth (at the end of the melting period). Thus, NDSI is evidently a better indicator of snow clearance in open areas than the employment of single-channel information, especially as it is also less sensitive to illumination geometry. In forest stand however, the indices showed stronger dependence on the illumination geometry. Single-channel approaches for the mapping of fractional snow cover, such as *SCAmod*, can be based on the application of scene reflectance models analogous to (3), which justifies the use of single-channel reflectance values instead of channel indices in the case of forested terrain.

The testing of NASA/GSFC SNOWMAP algorithm (Fig. 9) indicated that the method did not work ideally for the forest site under the

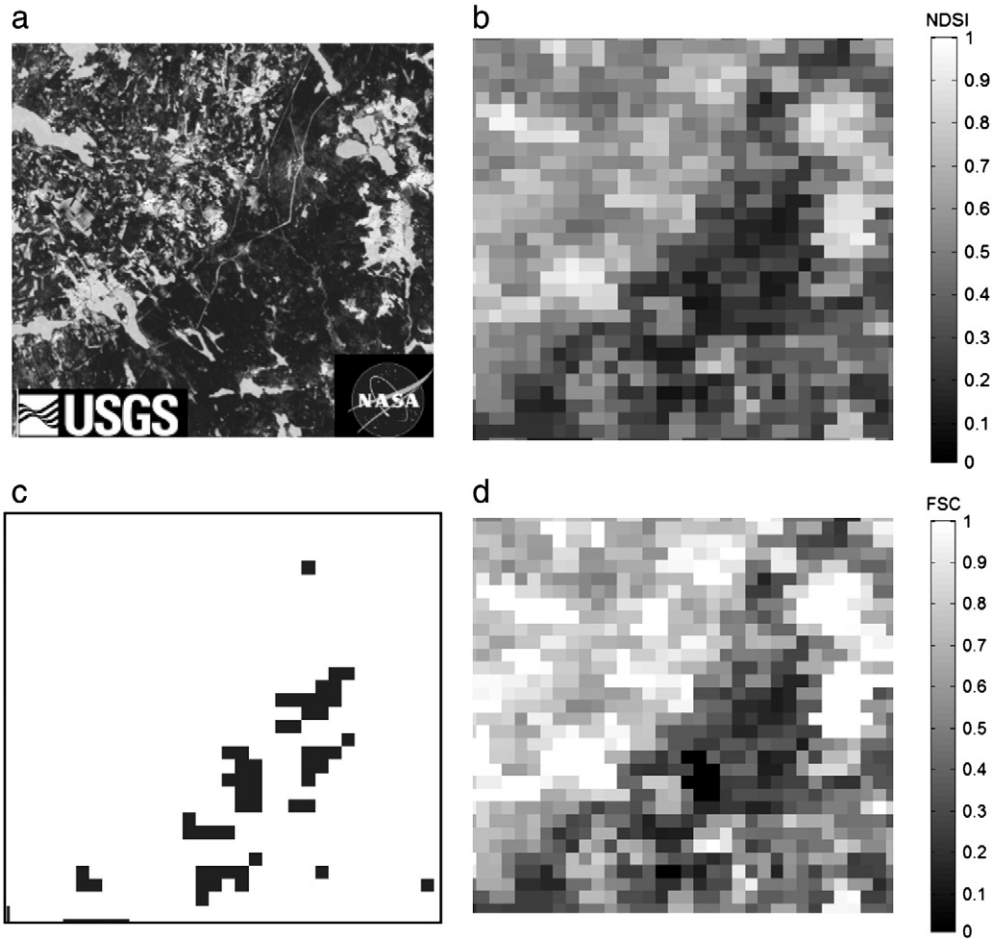

Fig. 11. The performance of MODIS snow mapping methods over fully snow-covered scene on 28 March 2003. a) A subset of Landsat/ETM+ scene on (15 March 2003), introducing the very dense forests, b) NDSI in MODIS 500 m-resolution, c) MOD10_L2 binary snow, white = snow, black = no snow, d) MOD10_L2 fractional snow.

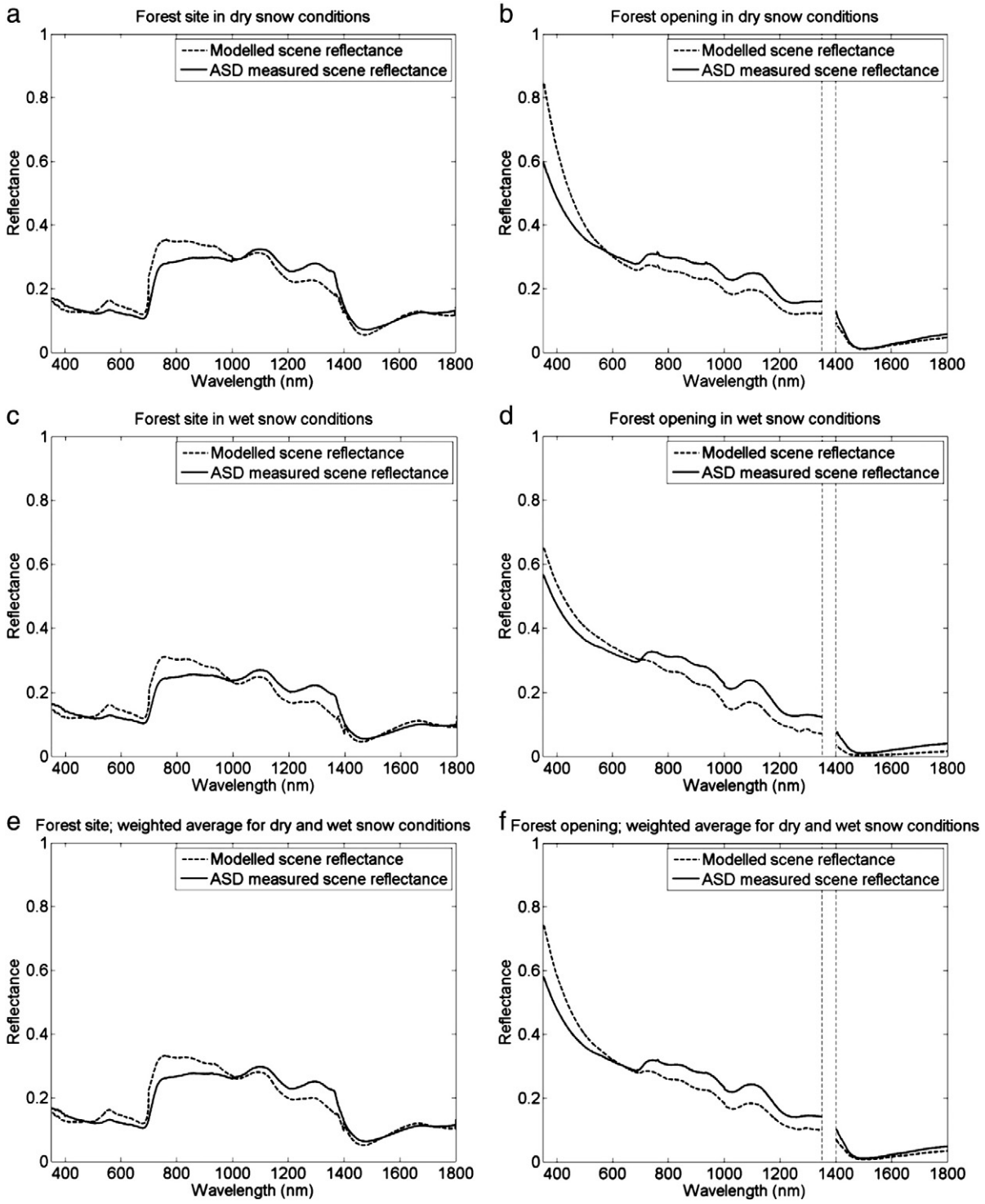

Fig. 12. Observed and modelled average scene spectra for the forest site (left) and the forest opening partially shadowed by trees (right). Both cases represent full snow cover conditions with direct illumination. Modelled spectra were determined using Eq. (3) for the forest area and Eq. (4) forest opening.

study (representing a typical boreal forest in Finland). The algorithm expects positive NDSI values for snow-covered terrain. However, negative NDSI (min. −0.15) were observed with full snow cover of depth over 70 cm. Here we used top of canopy observed reflectances for calculating NDSI. Accounting for the influence of atmosphere (i.e. the use of top-of-atmosphere reflectances) would slightly increase the level of NDSI from the values depicted in Figs. 9 and 10. However, according to our simulations, some negative values of NDSI from full snow-covered forest floor would still be present. This evidently occurs due to forest canopy effects. In addition, we demonstrated that low NDSI (<0.1 which is critical for the MODIS snow mapping method) is introduced also in the scale of MODIS 500 m-pixel, indicating that problems related to NDSI-based methods are relevant also in regional/continental scale snow mapping. Since NDSI has been found to be sensitive to the solar elevation, the further investigation of NDSI-based methodologies is highly important particularly in high latitudes where solar elevation is low during the snow season. Xin et al. (2012) have concluded that NDSI decreases

as view zenith angle increases. In this article the view zenith angle was stabile but NDSI introduced high variation, even within a day, which indicated that NDSI is highly dependent on solar position.

Comparison between the mast-observed and the modelled scene reflectances showed that forest transmissivity is dependent on wavelengths, as supported by other authors (e.g. Knipling, 1970; Woolley, 1971; Zarco-Tejada et al., 2004). A possible reason for the small modelling inaccuracy may be the spectrally changing reflection/transmission of incoming irradiance from/through the trees that surround the observed snow. This will be investigated in our future work. In general, the modelling approach combining linear mixing and radiative transfer models performed rather well. This was the case even though the viewing angle differed 11° between ground-based and mast-borne ASD measurements. This points out the feasibility of the applied model to predict the scene reflectance characteristics observed by space-borne or airborne instruments. The results also suggest that a radiative transfer approach is able to describe the light propagation and reflection effects of tree canopy better than a linear mixing approach.

Furthermore, the findings indicate some topics of further research concerning Earth Observation based snow monitoring. These include the study of spatial effects of forest canopy as well as the effects of prevailing conditions (illumination geometry and snow conditions) on reflectance and on SCA estimation algorithms. These issues will be tackled in the forthcoming research applying data from AISA (Airborne Imaging Spectroscopy) campaigns conducted in the Sodankylä site enabling the combined use of mast-borne, ground-based, airborne and satellite observation-derived reflectance data sets.

Acknowledgement

This work has been funded by the Airborne Imaging Spectroscopy Application and Research on Earth Sciences (AISARES) graduate school of the University of Helsinki.

References

Cao, Y. -G., & Liu, C. (2006). Normalized difference snow index simulation for snow-cover mapping in forest by geosail model. *Chinese Geographical Science*, *16*, 171–175.

Dozier, J., Green, R. O., Nolin, A. W., & Painter, T. H. (2009). Interpretation of snow properties from imaging spectrometry. *Remote Sensing of Environment*, *113*, S25–S37.

Eklundh, L., Jönsson, P., & Kuusk, A. (2007). Investigating modelled and observed Terra/MODIS 500-m reflectance data for viewing and illumination effects. *Advances in Space Research*, *39*, 119–124.

Gong, G., Cohen, J., Entekhabi, D., & Ge, Y. (2007). Hemispheric-scale climate response to Northern Eurasia land surface characteristics and snow anomalies. *Global and Planetary Change*, *56*, 359–370.

Gutman, G. G. (1991). Vegetation indices from AVHRR: An update and future prospects. *Remote Sensing of Environment*, *35*, 121–136.

Haefner, H., Seidel, K., & Ehrler, H. (1997). Applications of snow cover mapping in high mountain regions. *Physics and Chemistry of the Earth*, *22*, 275–278.

Hall, D. K., Riggs, G. A., & Salomonson, V. V. (1995). Development of methods for mapping global snow cover using moderate resolution imaging spectroradiometer data. *Remote Sensing of Environment*, *54*, 127–140.

Hall, D. K., Foster, J. L., Verbyla, D. L., Klein, A. G., & Benson, C. S. (1998). Assessment of snow-cover mapping accuracy in a variety of vegetation-cover densities in Central Alaska. *Remote Sensing of Environment*, *66*, 129–137.

Hall, D. K., Riggs, G. A., Salomonson, V. V., DiGirolamo, N. E., & Bayr, K. J. (2002). MODIS snow-cover products. *Remote Sensing of Environment*, *83*, 181–194.

Hall, D. K., & Riggs, G. A. (2007). Accuracy assessment of the MODIS snow products. *Hydrological Processes*, *21*, 1534–1547.

Hendriks, J., & Pellikka, P. (2004). Estimation of reflectance from a glacier surface by comparing spectrometer measurements with satellite-derived reflectances. *Zeitschrift für Gletscherkunde und Glazialgeologie*, *38*, 139–154.

Jylhä, K., Tuomenvirta, H., & Ruosteenoja, K. (2004). Climate change projections for Finland during the 21st century. *Boreal Environment Research*, *9*, 127–152.

Klein, A. G., Hall, D. K., & Riggs, G. A. (1998). Improving snow cover mapping in forests through the use of a canopy reflectance model. *Hydrological Processes*, *12*, 1723–1744.

Knipling, E. B. (1970). Physical and physiological basis for the reflectance of visible and near-infrared radiation from vegetation. *Remote Sensing of Environment*, *1*, 155–159.

Kuusisto, E. (1984). Snow accumulation and snowmelt in Finland. *Publications of the Water Research Institute*, *vol. 55*, Helsinki, Finland: National Board of Waters.

Marshall, S., & Oglesby, R. J. (1994). An improved snow hydrology for GCMs. Part 1: snow cover fraction, albedo, grain size, and age. *Climate Dynamics*, *10*, 21–37.

Mellander, P. -E., Loefvenius, M. O., & Laudon, H. (2007). Climate change impact on snow and soil temperature in boreal Scots Pine stands. *Climatic Change*, *85*, 179–193.

Mesarch, M. A., Walter-Shea, E. A., Asner, G. P., Middleton, E. M., & Chan, S. S. (1999). A revised measurement methodology for conifer needles spectral optical properties: evaluating the influence of gaps between elements. *Remote Sensing of Environment*, *68*, 177–192.

METLA (2010). *Finnish Statistical Yearbook of Forestry*. (pp. 62)Vammala, Finland: Finnish Forest Research Institute.

Metsämäki, S., Vepsäläinen, J., Pulliainen, J., & Sucksdorff, Y. (2002). Improved linear interpolation method for the estimation of snow-covered area from optical data. *Remote Sensing of Environment*, *82*, 64–78.

Metsämäki, S. J., Anttila, S. T., Markus, H. J., & Vepsäläinen, J. M. (2005). A feasible method for fractional snow cover mapping in boreal zone based on a reflectance model. *Remote Sensing of Environment*, *95*, 77–95.

Metsämäki, S., Mattila, O. -P., Pulliainen, J., Niemi, K., Luojus, K., & Böttcher, K. (2012). An optical reflectance model-based method for fractional snow cover mapping applicable to continental scale. *Remote Sensing of Environment*, http://dx.doi.org/10.1016/j.rse.2012.04.010.

Negi, H. S., Singh, S. K., Kulkarni, A. V., & Semwal, B. S. (2010). Field-based spectral reflectance measurements of seasonal snow cover in the Indian Himalaya. *International Journal of Remote Sensing*, *31*, 2393–2417.

Nolin, A. W., & Dozier, J. (2000). A hyperspectral method for remotely sensing the grain size of snow. *Remote Sensing of Environment*, *74*, 207–216.

Painter, T. H., Roberts, D. A., Green, R. O., & Dozier, J. (1998). The effect of grain size on spectral mixture analysis of snow-covered area from AVIRIS data. *Remote Sensing of Environment*, *65*, 320–332.

Painter, T. H., Dozier, J., Roberts, D. A., Davis, R. E., & Green, R. O. (2003). Retrieval of subpixel snow-covered area and grain size from imaging spectrometer data. *Remote Sensing of Environment*, *85*, 64–77.

Pellikka, P., & Rees, W. G. (2010). Glacier parameters monitored using remote sensing. In C. R. C. Press (Ed.), *Remote Sensing of Glaciers — techniques for topographic, spatial and thematic mapping of glaciers* (pp. 41–66). Leiden: Taylor & Francis Group.

Peltoniemi, J. I., Kaasalainen, S., Näränen, J., Rautiainen, M., Stenberg, P., Smolander, H., et al. (2005). BRDF measurement of understory vegetation in pine forests: dwarf shrubs, lichen, and moss. *Remote Sensing of Environment*, *94*, 343–354.

Rasmus, S. (2005). Snow Pack Structure Characteristics in Finland — Measurements and Modelling. *Department of Physical Sciences, Division of Geophysics* (pp. 244). Helsinki: University of Helsinki.

Riggs, G. A., Hall, D. K., & Salomonson, V. V. (2006). *MODIS Snow Product User Guide to Collection*, *5*, .

Salminen, M., Pulliainen, J., Metsamaki, S., Kontu, A., & Suokanerva, H. (2009). The behaviour of snow and snow-free surface reflectance in boreal forests: Implications to the performance of snow covered area monitoring. *Remote Sensing of Environment*, *113*, 907–918.

Salomonson, V. V., & Appel, I. (2004). Estimating fractional snow cover from MODIS using the normalized difference snow index. *Remote Sensing of Environment*, *89*, 351–360.

Salomonson, V. V., & Appel, I. (2006). Development of the Aqua MODIS NDSI fractional snow cover algorithm and validation results. *IEEE Transactions on Geoscience and Remote Sensing*, *44*, 1747–1756.

Solberg, R., & Andersen, T. (1994). An automatic system for operational snow-cover monitoring in the Norwegian mountain regions. *International Geoscience and Remote Sensing Symposium (IGARSS), 8–12 Aug 1994, Pasadena, CA, USA* (pp. 2084–2086).

Sukuvaara, T., Kyrö, E., Suokanerva, H., Heikkinen, P., & Suomalainen, J. (2007). Reflectance spectroradiometer measurement system in 30 meter mast for validating satellite images. *Proceedings of the IEEE 2007 International Geoscience and Remote Sensing Symposium (IGARSS), 23–27 July 2007, Barcelona Spain* (pp. 1524–1528).

Törmä, M., Härmä, P., Hatunen, S., Teiniranta, R., Kallio, M., & Järvenpää, E. (2011). Change detection for Finnish CORINE land cover classification. *SPIE, 20 September 2011 Prague, Czech Republic*.

Walter-Shea, E. A., Privette, J., Cornell, D., Mesarch, M. A., & Hays, C. J. (1997). Relations between directional spectral vegetation indices and leaf area and absorbed radiation in Alfalfa. *Remote Sensing of Environment*, *61*, 162–177.

Warren, S. G. (1982). Optical properties of snow. *Rewievs of Geophysics and Space Physics*, *20*, 67–89.

Vikhamar, D., & Solberg, R. (2003a). Snow-cover mapping in forests by constrained linear spectral unmixing of MODIS data. *Remote Sensing of Environment*, *88*, 309–323.

Vikhamar, D., & Solberg, R. (2003b). Subpixel mapping of snow cover in forests by optical remote sensing. *Remote Sensing of Environment*, *84*, 69–82.

Winther, J. -G., & Hall, D. K. (1999). Satellite-derived snow coverage related to hydropower production in Norway-present and future. *International Journal of Remote Sensing*, *20*, 2991–3008.

Woolley, J. T. (1971). Reflectance and transmittance of light by leaves. *Plant Physiology*, *47*, 656–662.

Xin, Q. C., Woodcock, C. E., Liu, J. C., Tan, B., Mellohd, R. A., & Davis, R. E. (2012). View angle effects on MODIS snow mapping in forests. *Remote Sensing of Environment*, *118*, 50–59.

Zarco-Tejada, P. J., Miller, J. R., Harron, J., Hu, B., Noland, T. L., Goel, N., et al. (2004). Needle chlorophyll content estimation through model inversion using hyperspectral data from boreal conifer forest canopies. *Remote Sensing of Environment*, *89*, 189–199.